Received: 26 September 2022 | Revised: 21 March 2023 | Accepted: 8 April 2023

DOI: 10.1002/hbm.26315

RESEARCH ARTICLE

WILEY

Cerebral blood flow patterns in preterm and term neonates assessed with pseudo-continuous arterial spin labeling perfusion MRI

Eleonora Piccirilli[1,2] | Antonio M. Chiarelli[1,2] | Carlo Sestieri[1,2] | Daniele Mascali[1,2] | Darien Calvo Garcia[1,2] | Adele Primavera[3] | Rita Salomone[3] | Richard G. Wise[1,2] | Antonio Ferretti[1,2] | Massimo Caulo[1,2,4]

[1]Department of Neuroscience, Imaging, and Clinical Sciences, University G. d'Annunzio of Chieti-Pescara, Chieti, Italy

[2]Institute for Advanced Biomedical Technologies (ITAB), University G. d'Annunzio of Chieti-Pescara, Chieti, Italy

[3]Department of Paediatrics, Neonatology and Neonatal Intensive Care Unit, University Hospital of Chieti, Chieti, Italy

[4]Department of Radiology, SS. Annunziata Hospital, Chieti, Italy

Correspondence
Massimo Caulo, Department of Neuroscience, Imaging and Clinical Sciences, Institute for Advanced Biomedical Technologies, University G. d'Annunzio of Chieti-Pescara, Chieti, Italy.
Email: massimo.caulo@unich.it

Funding information
Departments of Excellence 2018-2022, Italian Ministry of Education, University and Research

Abstract

In preterm (PT) infants, regional cerebral blood flow (CBF) disturbances may predispose to abnormal brain maturation even without overt brain injury. Therefore, it would be informative to determine the spatial distribution of grey matter (GM) CBF in PT and full-term (FT) newborns at term-equivalent age (TEA) and to assess the relationship between the features of the CBF pattern and both prematurity and prematurity-related brain lesions. In this prospective study, we obtained measures of CBF in 66 PT (51 without and 15 with prematurity-related brain lesions) and 38 FT newborns through pseudo-continuous arterial spin labeling (pCASL) MRI acquired at TEA. The pattern of GM CBF was characterized by combining an atlas-based automated segmentation of structural MRI with spatial normalization and hierarchical clustering. The effects of gestational age (GA) at birth and brain injury on the CBF pattern were investigated. We identified 4 physiologically-derived clusters of brain regions that were labeled Fronto-Temporal, Parieto-Occipital, Insular-Deep GM (DGM) and Sensorimotor, from the least to the most perfused. We demonstrated that GM perfusion was associated with GA at birth in the Fronto-Temporal and Sensorimotor clusters, positively and negatively, respectively. Moreover, the presence of periventricular leukomalacia was associated with significantly increased Fronto-Temporal GM perfusion and decreased Insular-DGM perfusion, while the presence of germinal matrix hemorrhage appeared to mildly decrease the Insular-DGM perfusion. Prematurity and prematurity-related brain injury heterogeneously affect brain perfusion. ASL MRI may, therefore, have strong potential as a noninvasive tool for the accurate stratification of individuals at risk of domain-specific impairment.

Abbreviations: CBF, cerebral blood flow; FT, full-term; GA, gestational age; GM, grey matter; GMH, germinal matrix hemorrhage; $nCBF_{GM}$, normalized CBF of the grey matter; pCASL, pseudocontinuous arterial spin labeling; PT, preterm; PVL, periventricular leukomalacia; ROI, region of interest.

Eleonora Piccirilli and Antonio M. Chiarelli contributed equally to this work.

KEYWORDS
arterial spin labeling (ASL), brain injury, cerebral blood flow (CBF), pattern analysis, premature neonates

1 | INTRODUCTION

The intensive and long-lasting maturation during the second half of pregnancy exposes the brain to the risk of injuries, especially in preterm (PT) neonates (Padilla et al., 2015). The early exposure to extrauterine life and external stimuli as well as the artificial environment of the neonatal intensive care unit are known to affect brain maturation (Lubsen et al., 2011). The risk of neurodevelopmental impairment is inversely related to gestational age (GA) at birth and deficits are more common and severe in the presence of periventricular leukomalacia (PVL) and germinal matrix hemorrhage (GMH) (Woodward et al., 2012). However, motor and cognitive deficits have been demonstrated in the absence of overt brain injury (Bouyssi-Kobar et al., 2016). Although their exact etiological mechanisms have not been completely elucidated (Bouyssi-Kobar et al., 2016), there is growing evidence that disturbances in CBF may predispose to abnormal brain maturation, making CBF an important biomarker of brain functional development (Fyfe et al., 2014).

Given the potential link between disturbances of brain perfusion and poor neurodevelopmental outcomes in PT babies, several studies attempted to evaluate CBF in this population with arterial spin labeling (ASL), reporting CBF abnormalities at both global and regional levels (Bouyssi-Kobar et al., 2018; De Vis et al., 2013; Mahdi et al., 2018; Ouyang et al., 2017; Tortora et al., 2017; Zun et al., 2021). However, a crucial limitation of previous studies concerns regional specificity. In some studies, regions of interest (ROI)s were manually drawn, potentially resulting in operator-dependent biases, low reliability and excessive focus on specific structures (Bouyssi-Kobar et al., 2018; Kim et al., 2018). In other studies employing automatic segmentation, the analysis was performed considering either the cortex as a whole or coarse anatomical boundaries to define few brain regions, without accounting for their functional characteristics and potentially failing to identify the effect of prematurity on spatially distributed patterns of CBF (Tortora et al., 2017; Zun et al., 2021).

Based on previous reports, we hypothesize that CBF distributes differently between full-term (FT) and PT infants. In addition, we predict the presence of a relationship between the features of the CBF pattern and both the GA at birth and the presence of PVL and GMH. To test these hypotheses, in the present study, we characterized the regional distribution of grey matter $CBF_{(GM)}$ in neonates at term-equivalent age (TEA). By combining automated segmentation algorithms of structural MR images and a data-driven hierarchical clustering on ASL perfusion maps, we assessed and compared the CBF_{GM} patterns between FT and PT newborns, and evaluated their modifications with GA at birth and prematurity-related brain lesions.

2 | MATERIALS AND METHODS

2.1 | Population

This prospective observational study was approved by the local ethical committee of the University G. D'Annunzio of Chieti-Pescara, Chieti, Italy and was conducted in accordance with the declaration of Helsinki. Written informed consent was obtained from each infant's parents. A total of 72 PT (GA at birth < 37 weeks) and 51 FT (GA at birth ≥ 37 weeks) from the Neonatology Unit of the University Hospital of Chieti were recruited from 2017 to 2021. Seventy-seven newborns were delivered via C-section. PT with major neonatal morbidity (severe respiratory distress syndrome, bronchopulmonary dysplasia, necrotizing enterocolitis, patent ductus arteriosus, and sepsis) were not included. PT were also screened for the presence of GMH and PVL. Healthy PT were further subdivided into three categories on the basis of their GA at birth as defined by the World Health Organization (WHO) classification (World Health Organization, 2012): Early (PT_{HE}: ≤28 weeks), Moderate (PT_{HM}: 29–32 weeks) and Late PT (PT_{HL}: 33–36 weeks) (refer to Section 3.1 for numerosity).

The FT cohort consisted of infants with uneventful deliveries that underwent MRI because of symmetrical and bilateral periventricular white matter increased echogenicity at early routine cranial ultrasound. However, no FT infant included in the study showed evidence of brain lesion at MRI, consistently with the reported paraphysiological nature of this type of increased echogenicity (Leijser et al., 2009). For both cohorts, exclusion criteria were: perinatal asphyxia, brain lesions at MRI (other than prematurity-related lesions), chromosomal/genetic abnormalities, congenital malformations, brain infections, metabolic disorders, and hydrocephalus.

Written medical records were reviewed extracting the following demographics and clinical variables: GA at birth, birth weight, sex, APGAR score at 1 and 5 min.

2.2 | MRI acquisition

Newborns underwent the MRI protocol on a 3T scanner (Philips Achieva, Best, The Netherlands) using a 32-channel head coil, between the 40th and the 42nd week of post menstrual age (PMA, i.e., at TEA). Infants were fed and sedated with one administration of intranasal Midazolam (0.05 mg/kg of body weight) prior to acquisition. Heart rate and oxygen saturation were continuously monitored during image acquisition by an intensive care neonatologist.

The clinical MRI protocol included 3D T1-weighted, axial and coronal T2-weighted (T2WI), diffusion-weighted (DWI), and susceptibility-weighted (SWI) images. For the present study, we only analyzed the

axial T2WI (resolution = 0.4 × 0.4 × 3.5 mm^3, FOV = 204 × 204 × 98 mm^3). In addition to the clinical protocol, ASL was acquired for CBF evaluation with a pseudo-continuous ASL (pCASL) sequence consisting of 4 paired tag-control volumes measured with a 4 segment multi-shot 3D Gradient and Spin Echo (GRaSE) readout and background suppression (TE = 24 ms, TR = 4.4 s, resolution = 2.5 × 2.5 × 7 mm^3, FOV = 200 × 200 × 91 mm^3). Labeling duration (τ) and post-label delay (PLD) were 1.8 s and 2 s, respectively, following guidelines on ASL acquisition in neonates from Alsop et al. (Alsop et al., 2015). The labeling plane was centered over the neck, perpendicular to the main cerebro-afferent arteries, and the imaging-labeling plane gap ranged from 10 to 20 mm. A fast TOF MR angiography centered over the neck was acquired to delineate the course of the cerebro-afferent arteries. Magnetization at rest (M_0) was also acquired using the pCASL sequence without labeling and background suppression. The total acquisition time was 20 min, while the duration of the ASL sequence was 3.15 min.

2.3 | Evaluation of brain injury

All images were reviewed by a neuroradiologist (EP) for evidence of radiological exclusion criteria and prematurity-related parenchymal brain injury (GMH and PVL). PVL was assessed according to the Kidokoro score (Kidokoro et al., 2014) and GMH was graded following the modified Papile classification (Mukerji et al., 2015). PT infants were stratified into those without (PT_H, further divided in PT_{HE}, PT_{HM}, PT_{HL}) and those with prematurity-related brain injury (PT_{PVL} and PT_{GMH}, respectively).

2.4 | Cerebral blood flow computation

The axial T2WI and the University of North Carolina (UNC) Infant Atlas for neonates (Avants et al., 2011; Shi et al., 2011) were used for segmentation purposes and for delineating regions of interest (ROIs). pCASL analysis was performed with a combination of FSL (FMRIB, Oxford, UK), dHCP pipeline, ANTS, and Matlab (Avants et al., 2009; Jenkinson et al., 2012; Makropoulos et al., 2018). The pre-processing steps included: motion correction with M_0 as reference using MCFLIRT from FSL, T2WI, and M_0 brain extraction using BET from FSL, T2WI brain segmentation using the dHCP pipeline, T2 brain co-registration to M_0 brain using FLIRT from FSL and the UNC Infant Atlas warping into M_0 brain using antsRegistrationSyN from ANTS.

CBF (in quantitative units) was obtained by averaging the 4 tag-control difference images (ΔM), by using voxel-wise M_0 normalization and the single-compartment PCASL kinetic model:

$$CBF = \frac{6000 \cdot \lambda \cdot e^{\frac{PLD}{T1_b}}}{\alpha \cdot \alpha_{inv} \cdot T1_b \cdot \left(1 - e^{-\frac{\tau}{T1_b}}\right)} \cdot \left(\frac{\Delta M}{M_0}\right) \text{mL/100g/min} \quad (1)$$

with a brain/blood partition coefficient $\lambda = 0.9$ mL/g, labeling efficiency $\alpha = .85$, labeling efficiency reduction due to background suppression $\alpha_{INV} = .88$ and T1 of blood $T1_b = 1.67$ s (Alsop et al., 2015).

The T2WI segmentation yielded masks of the cortical and deep GM. The T2WI, its GM segmentation and the UNC Infant Atlas were transformed into the pCASL space. The quality of the registration was visually assessed by EP. Regional CBF_{GM} was then extracted from the 90 ROIs of the UNC Infant Atlas. The CBF_{GM} expressed in quantitative units was only used to qualitatively assess single subject CBF maps. In fact, CBF quantitative computation is strongly affected by the $T1_b$ (Equation (1)) which linearly dependent on hematocrit (De Vis et al., 2014). The hematocrit is highly variable in newborns (especially PT) and the hematocrit at the time of MRI scans was not available for all infants, nor a quantitative evaluation of $T1_b$ through MRI sequences was available. This strong variability across participants hampered the possibility to perform comparisons of quantitative CBF across subjects or groups.

A CBF_{GM} pattern analysis across subjects was performed by normalizing the CBF maps through spatial z-scoring (among the 90 ROIs): the normalized CBF_{GM} ($nCBF_{GM}$) for each ROI represented the distance, in units of standard deviation (SD), from the subject's average CBF_{GM}. The analysis of $nCBF_{GM}$ allowed to address how CBF was spatially distributed, independently of its absolute value.

2.5 | Hierarchical clustering

To reduce the number of brain regions from the 90 ROIs and increase the study power and interpretability, a data-driven hierarchical clustering of ROIs was performed using the Ward's method (Ward Jr, 1963). The optimal number of clusters from the cluster tree was derived using the "elbow method" (Robert, 1953).

Importantly, the hierarchical clustering was performed exploiting physiological information, using the $nCBF_{GM}$ across PT_H and FT (creating the feature space) and ROIs (considered as samples). The clustering stability was assessed using a bootstrap approach (random sampling with replacement of newborns) with 10,000 iterations, and by counting the number of times each ROI was not included in the cluster to which it was attributed using the complete data set (Hesterberg, 2011).

2.6 | Statistical analysis

Normality distribution of variables was evaluated using the Kolmogorov–Smirnov test. Multiple one-way ANOVAs were performed for evaluating differences in $nCBF_{GM}$ among three groups of PT_H (PT_{HE}, PT_{HE}, PT_L) and FT in each cluster identified by the hierarchical clustering. Multiple one-way ANOVAs were also computed within each cluster to evaluate differences in $nCBF_{GM}$ among PT_H, PT_{PVL}, and PT_{GMH}; the within-group variability associated with GA at birth was accounted for in the latter analysis by regressing out GA at birth based on its association with $nCBF_{GM}$ within the PT_H. $nCBF_{GM}$ outliers in each group (defined as values above or below 2SD from the mean) were excluded from the

ANOVAs when normality assumption was not met. Unpaired *t*-tests were performed for post-hoc analysis, with a control for multiple comparison if needed (using false discovery rate, FDR). Pairwise associations between variables were assessed using Pearson's linear correlation. A $p < .05$ was considered statistically significant whereas a $p < .1$ was considered a trend towards significance. Statistical analysis was performed in Matlab (version R2020b).

3 | RESULTS

3.1 | Cohort characteristics

Figure 1 shows the flow-chart of infants enrollment and exclusion criteria. A total of 123 infants (72 PT and 51 FT) were enrolled and scanned. Within the 72 PT, 5 were excluded due to motion artifacts or poor quality of pCASL and 1 due to venous stroke. Among the remaining 66 PT, 51 had structurally normal brain MRI (PT_H) while 15 had brain injury related to prematurity. The division of the 51 PT_H on the basis of their GA at birth (see Materials and Methods section for more details) identified 9 PT_{HE}, 21 PT_{HM}, and 21 PT_{HL}. Of the 15 PT with brain injuries, 7 had mild–moderate PVL (PT_{PVL}, grades I–II of the Kidokoro score) and 8 had mild–moderate GMH (PT_{GMH}, grades I–II of the Papile score); none of the PT was found to have severe PVL or GMH. Of the 51 FTs, 7 were excluded due to motion artifacts/poor quality of pCASL, 4 due to metabolic and genetic conditions, and 2 due to arterial ischemic stroke, leaving a final group of 38 FT. Table 1 shows the characteristics of the 104 studied infants (66 PT and 38 FT).

3.2 | MRI pre-processing outcome

Figure 2 reports exemplar axial slices of the CBF map derived from the pCASL acquisition (Figure 2a), of the T2WI (Figure 2b) and of the UNC Infant Atlas (Shi et al., 2011) warped and overlaid onto the T2WI (Figure 2c).

3.3 | Grey matter perfusion distribution in healthy neonates and hierarchical clustering of perfusion pattern

Figure 3 reports the $nCBF_{GM}$ computed in the 90 ROIs of the UNC Infant Atlas including the 89 healthy neonates of the study (51 PT_H and 38 FT) and superimposed over the Atlas template.

The hierarchical clustering on the $nCBF_{GM}$, grouping the 90 ROIs of the Atlas into successively larger clusters, generated the dendrogram reported in the Supplementary Material (Figure S1). Four main clusters were identified explaining 70% of the between ROIs total $nCBF_{GM}$ variance.

Figure 4 reports the 4 color-coded clusters on the Atlas template. The first cluster (green), named *Fronto-Temporal*, was mainly formed by associative regions of the prefrontal (orbito-frontal cortex, superior, middle, and inferior frontal gyrus) and temporal (temporal pole, middle temporal gyrus, fusiform gyrus) cortex. The second cluster (cyan), named *Parieto-Occipital*, included associative regions of the parietal lobe, the calcarine cortex and structures of the limbic system (amygdalae, hippocampi, parahippocampal gyri). The third cluster (purple), named *Insular-DGM*, consisted of the insulae, the deep GM (DGM) nuclei and the thalami, and the Heschl gyri (primary auditory

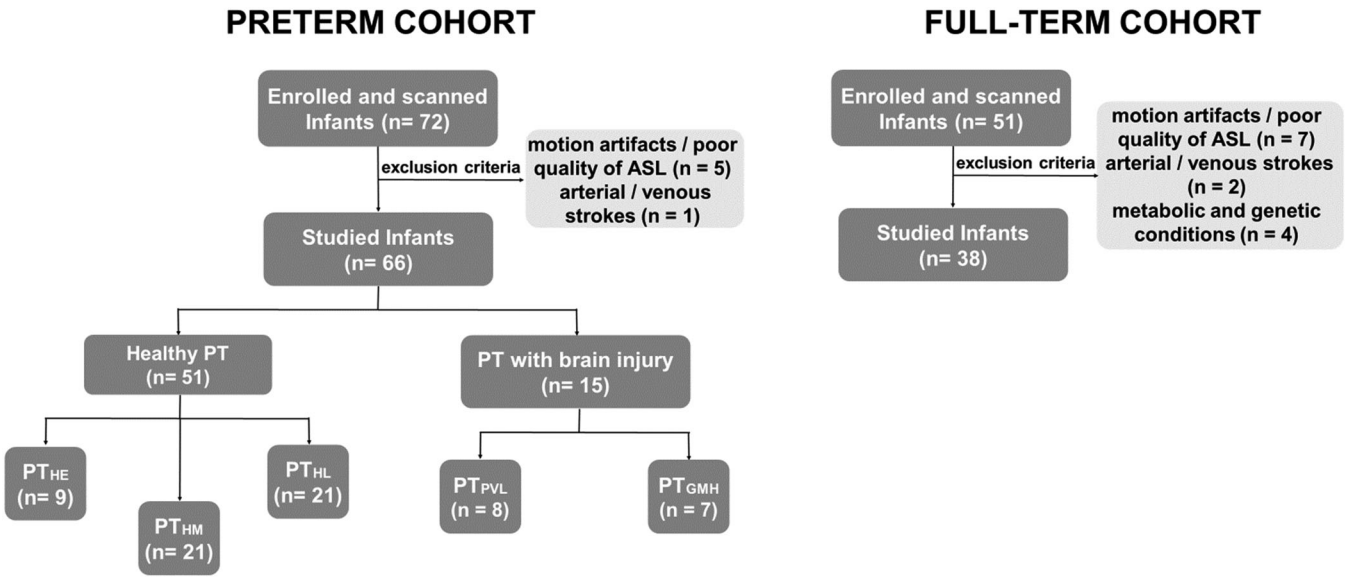

FIGURE 1 Flow-chart of neonates' enrollment and exclusion criteria. FT, full-term; PT, preterm; PT_{HE}, healthy early preterm; PT_{HM}, healthy moderate preterm; PT_{HL}, healthy late preterm; PT_{GMH}, preterm with germinal matrix hemorrhage; PT_{PVL}, preterm with periventricular leukomalacia.

TABLE 1 Demographic and clinical characteristics of the neonates that completed the study.

Characteristic	Healthy neonates ($N = 89$)				
	Healthy preterm (PT_H, $N = 51$)				
	Healthy early preterm (PT_{HE})	Healthy moderate preterm (PT_{HM})	Healthy late preterm (PT_{ML})	Full-term (FT)	*p*-value (one-way ANOVA)
N	9	21	21	38	-
Male/female ratio	7/2	13/8	10/11	21/38	$p =$ n.s.
GA at birth ± SD, range (weeks)	26.8 ± 1.4 (24–28)	30.4 ± 0.81 (29–32)	34.2 ± 1.5 (33–36)	39 ± 1.2 (37–41)	$p < 10^{-4}$****
PMA at scan ± SD (weeks)	40.5 ± 0.5	40.5 ± 0.6	40.5 ± 0.5	40.6 ± 0.8	$p =$ n.s.
Birth weight ± SD (g)	1066 ± 266	1397 ± 315	1790 ± 574	3226 ± 477	$p < 10^{-4}$****
APGAR score, 1′ ± SD	6 ± 1.58	5.78 ± 1.63	6.62 ± 1.88	6.42 ± 2.48	$p =$ n.s.
APGAR score, 5′ ± SD	8.11 ± 0.78	7.92 ± 0.73	8.17 ± 0.93	8.20 ± 1.54	$p =$ n.s.

Characteristic	Preterm (PT, $N = 66$)			
	Healthy preterm (PT_H)	Preterm with PVL (PT_{PVL})	Preterm with GMH (PT_{GMH})	*p*-Value (one-way ANOVA)
N	51	7	8	-
Male/female ratio	31/20	4/7	4/8	$p =$ n.s.
GA at birth ± SD, range (weeks)	30.9 ± 2.6 (24–37)	30.6 ± 1.13 (29–32)	30.8 ± 2.99 (27–35)	$p =$ n.s.
PMA at scan ± SD (weeks)	40.5 ± 0.4	40.5 ± 0.5	40.5 ± 0.6	$p =$ n.s.
Birth weight ± SD (g)	1505 ± 513	1521 ± 546	1493 ± 373	$p =$ n.s.
APGAR score, 1′ ± SD	6.19 ± 1.75	6.07 ± 2.20	7 ± 1.53	$p =$ n.s.
APGAR score, 5′ ± SD	8.07 ± 0.81	7.41 ± 1.73	8.50 ± 0.54	$p < 10^{-3}$***

$p < 10^{-3}$.*$p < 10^{-4}$.

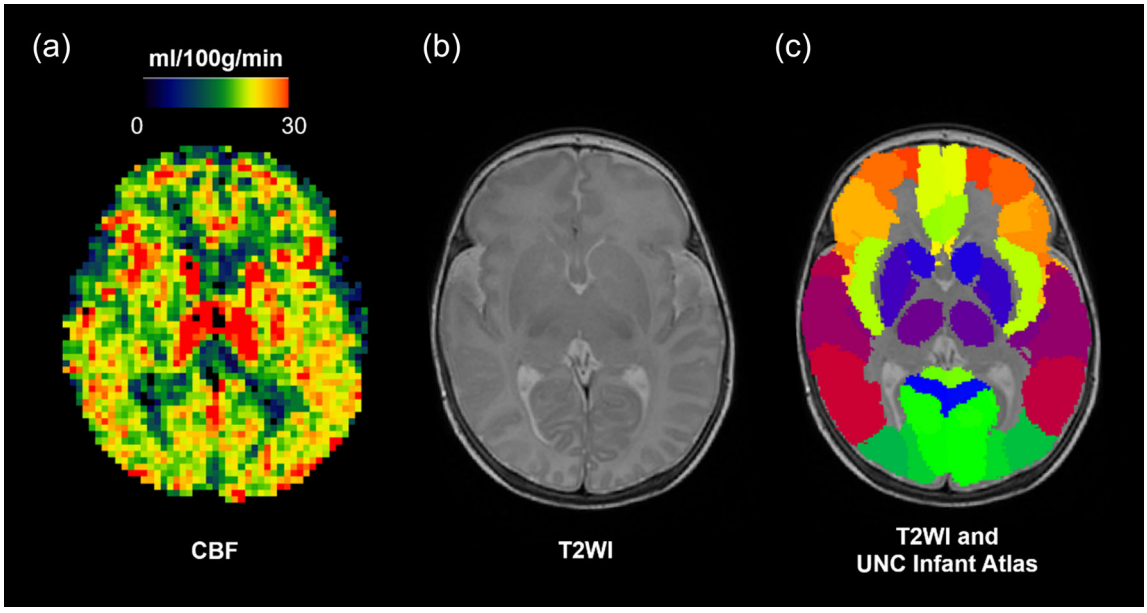

FIGURE 2 Exemplar axial slice of (a) cerebral blood flow (CBF) map derived from the pseudocontinuous arterial spin labeling (pCASL) acquisition; (b) T2-weighted (T2WI); (c) University of North Carolina (UNC) Infant Atlas warped and overlaid onto the T2WI. All images were acquired on the same FT neonate and are displayed in neurological convention.

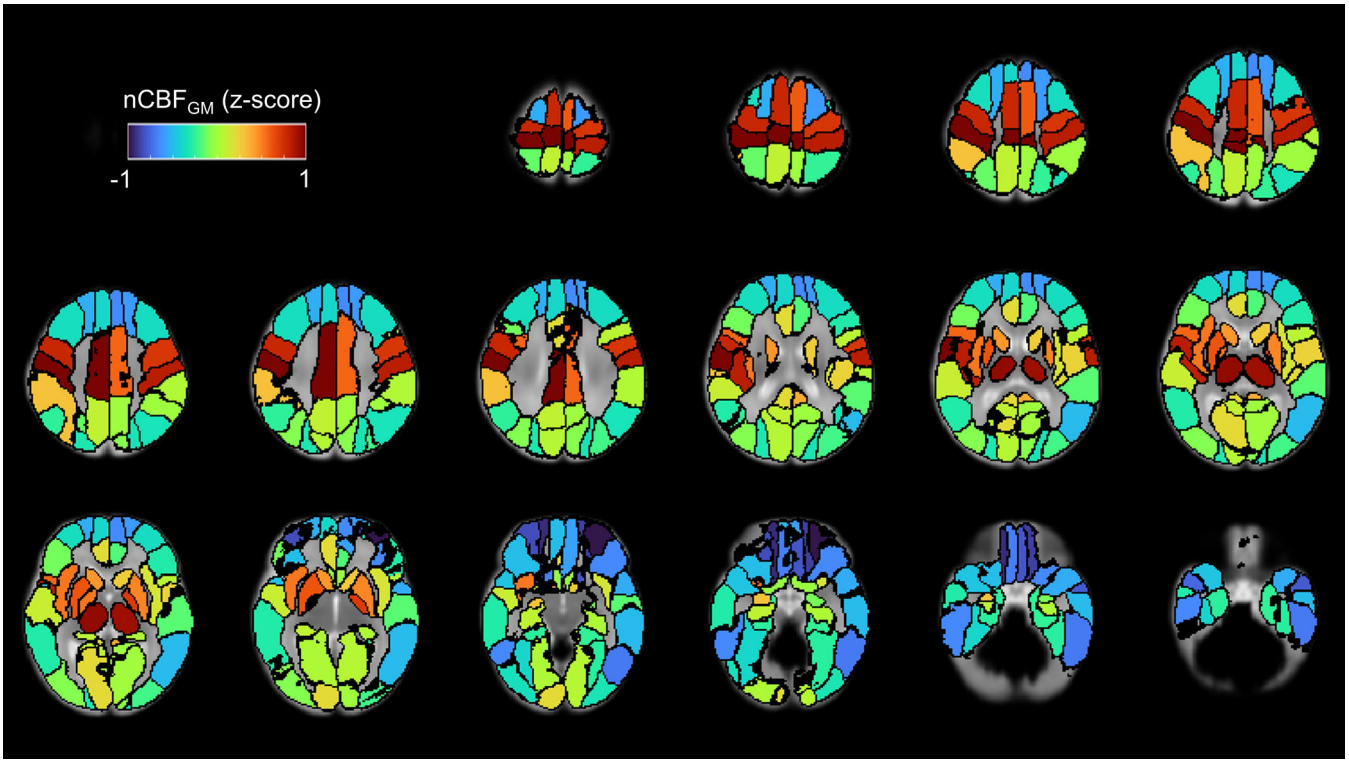

FIGURE 3 Average nCBF$_{GM}$ within the 90 ROIs of the University of North Carolina (UNC) Infant Atlas. Maps were computed considering all the healthy neonates of the study (PT$_H$ and FT). nCBF$_{GM}$ in each ROI and for each subject was computed as the distance, in units of standard deviation (SD), from the global CBF$_{GM}$ (average CBF$_{GM}$ between the 90 ROIs, z-score). Images are displayed in neurological convention.

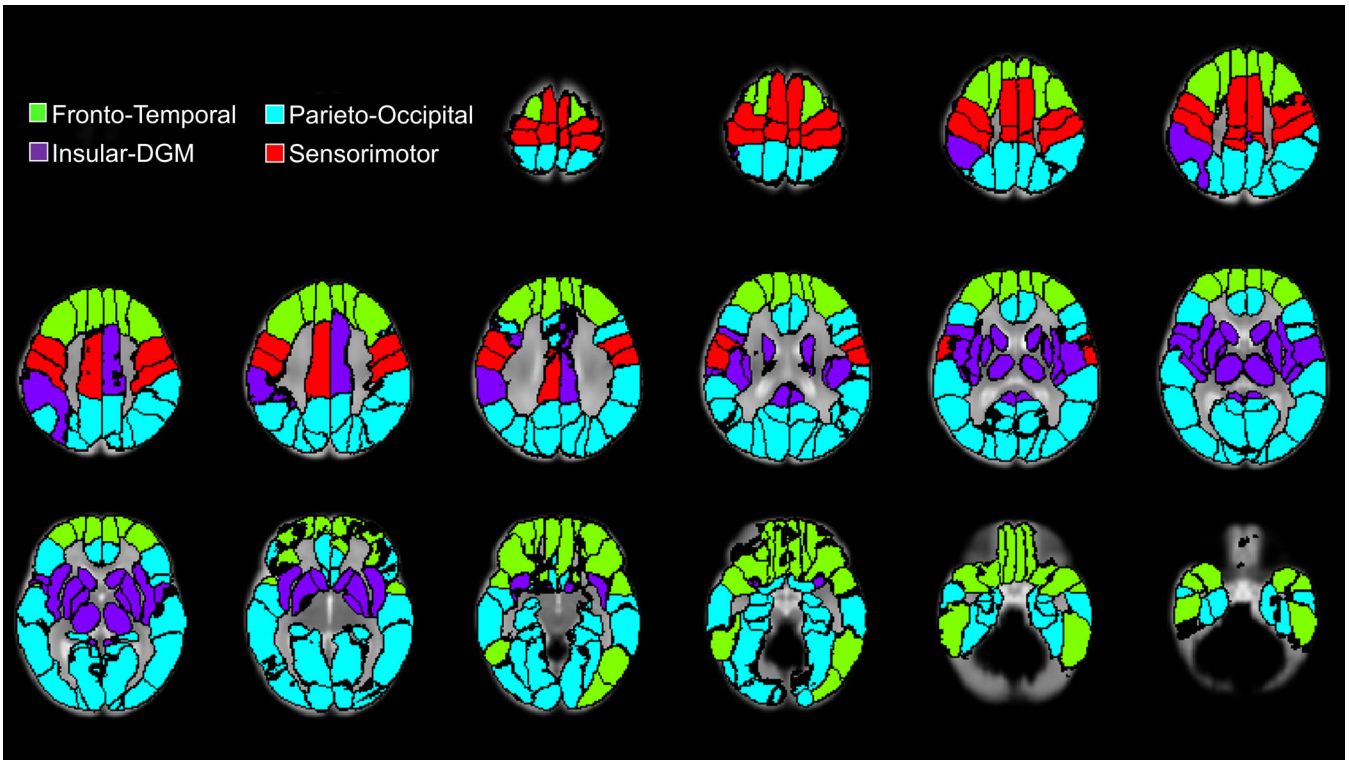

FIGURE 4 The 4 clusters identified by the hierarchical clustering using normalized CBF of the grey matter (nCBF$_{GM}$) in healthy neonates and reported on the template of the University of North Carolina (UNC) Infant Atlas. Images are displayed in neurological convention.

cortex). The fourth cluster (red), named *Sensorimotor*, included the peri-Rolandic cortices (pre and post-central gyri, primary somatomotor and somatosensory areas) and the supplementary motor areas.

Of note, the bootstrap analysis showed that, on average, in only 7% of the iterations the ROIs were not attributed to the same clusters reported in Figure 4, depicting the stability of the results. The only ROI showing a large percentage of misclassification (91%) was the right middle cingulate gyrus, thus, suggesting that this ROI was erroneously attributed to the insular-DMG cluster whereas probably it belonged to the sensorimotor cluster.

We observed high $nCBF_{GM}$ (i.e., z-scored CBF compared to 0) in the *Sensorimotor* and *Insular-DMG* clusters (0.94 ± 0.62, $p < 10^{-4}$ and 0.48 ± 0.26, $p < 10^{-4}$, respectively), average $nCBF_{GM}$ in the parieto-occipital cluster (−0.10 ± 0.15, $p =$ n.s.) and low $nCBF_{GM}$ in the *Fronto-Temporal* cluster (−0.62 ± 0.24, $p < 10^{-4}$).

3.4 | Intergroup comparison of perfusion pattern among healthy neonates

Figure 5 reports violin plots of $nCBF_{GM}$ measured separately for each cluster in 4 groups of healthy neonates, PT_{HE}, PT_{HM}, PT_{HL} and FT. For completeness, a correlation analysis is also reported for each cluster, evaluating the association between $nCBF_{GM}$ and GA at birth.

The one-way ANOVAs identified significant differences among the 4 groups in the *Fronto-Temporal* ($p < .01$) and *Sensorimotor* ($p < 10^{-3}$) clusters. In the *Fronto-Temporal* cluster $nCBF_{GM}$ was higher in FT as compared to all the PT_H subgroups (FT vs. PT_{HE}, $p < .01$, p with false discovery rate correction, pFDR, <.05; FT vs. PT_{HM}, $p < .05$, pFDR <.05; FT vs. PT_{HL} p < 0.05, pFDR <.05). A positive association was observed between $nCBF_{GM}$ and GA at birth ($r = .37$, $p < .01$). In the *Sensorimotor* cluster $nCBF_{GM}$ was lower in FT as compared to PT_{HE} ($p < 10^{-3}$,

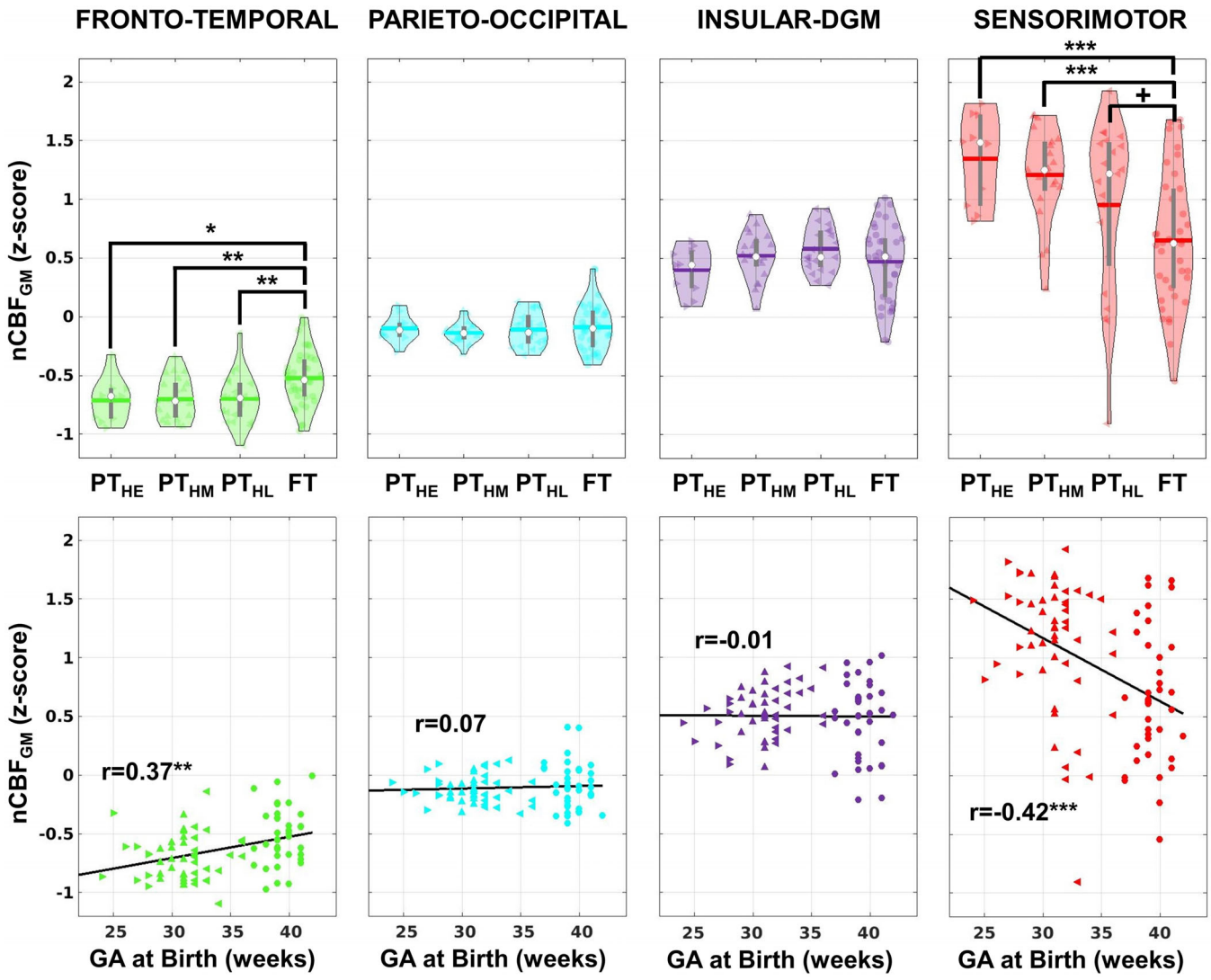

FIGURE 5 Violin plots of $nCBF_{GM}$ in PT_{HE}, PT_{HM}, PT_{HL}, and FT (upper row) as well as correlation analyses evaluating the association between $nCBF_{GM}$ and GA at birth (lower row). Data are reported for the 4 clusters identified by the hierarchical clustering. In the plots neonates in the different groups are identified by arrows with different orientations (PT) and dots (FT), CBF, cerebral blood flow; FT, full-term; GA, gestational age; nCBFGM normalized CBF of the grey matter; PT, preterm; PT_{HE}, healthy early preterm; PT_{HM}, healthy moderate preterm; PT_{HL}, healthy late preterm; PT_{GMH}, preterm with germinal matrix hemorrhage; PT_{PVL}, preterm with periventricular leukomalacia. $^{+}p < .1$. $^{*}p < .05$; $^{**}p < .01$; $^{***}p < 10^{-3}$.

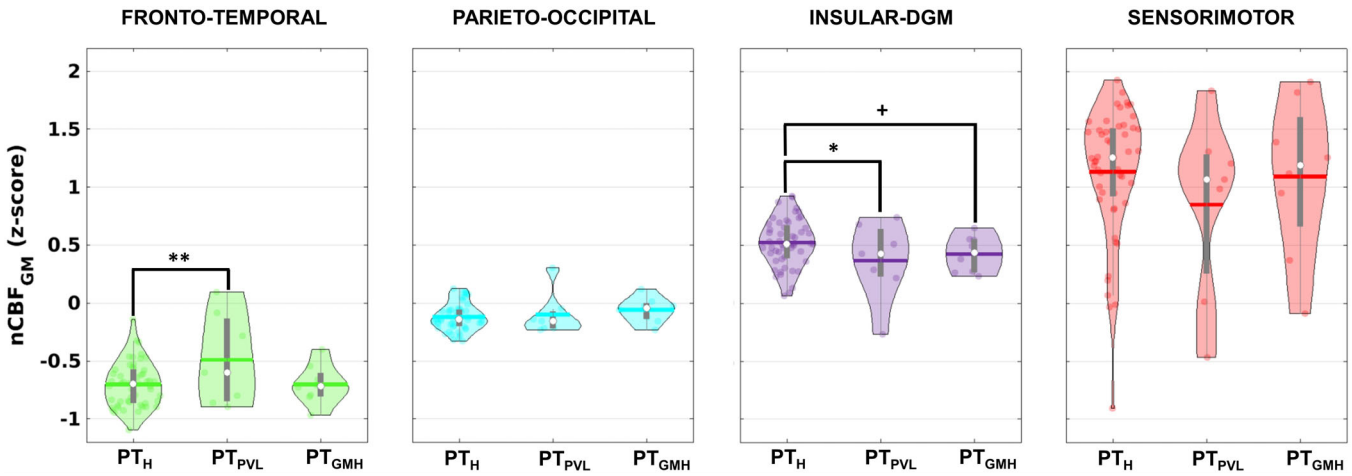

FIGURE 6 Violin plots of $nCBF_{GM}$ in PT_H, PT_{PVL}, PT_{GMH}. Data are reported for the 4 clusters identified by the hierarchical clustering. GA, gestational age; $PT_{H,}$ healthy preterm PT_{GMH}, preterm with germinal matrix hemorrhage; PT_{PVL}, preterm with periventricular leukomalacia. $^{+}p < .1$; $^{*}p < .05$; $^{**}p < .01$. Effect of GA at birth is accounted for.

*p*FDR <.01) and to PT_{HM} ($p < 10^{-3}$, *p*FDR <.01) and tended towards a significant lower value in FT compared to PT_{HL} ($p < .1$, pFDR = n.s.). A significant negative association was observed between $nCBF_{GM}$ and GA at birth ($r = -.42$, $p < 10^{-3}$). No differences in $nCBF_{GM}$ with GA at birth were identified in the *Parieto-Occipital* and *Insular-DMG* clusters. The associations between $nCBF_{GM}$ and GA at birth were evaluated without covarying out the demographic or clinical data. In fact, the only variable available which was associated with $nCBF_{GM}$ was weight at birth which had an extremely high correlation with GA at birth ($r = .90$, $p < 10^{-39}$), essentially encoding the same information. Of note the ability of the clustering approach to summarize ROI-based analyses was confirmed by the results of the ROI-wise correlations that are reported in the Supplementary Material (Figure S3).

3.5 | Intergroup comparison of perfusion pattern between healthy and premature neonates with brain injuries

Figure 6 reports violin plots of $nCBF_{GM}$ for the 4 clusters in 3 groups of PT with and without brain injuries (PT_H, PT_{PVL}, PT_{GMH}). The one-way ANOVAs identified significant differences among the 3 groups in the *Fronto-Temporal* ($p < .05$) and *Insular-DMG* ($p < .05$) clusters (accounting for the possible confounding effect of GA at birth). In the *Fronto-Temporal* cluster, $nCBF_{GM}$ was higher in PT_{PVL} than in PT_H ($p < .05$, *p*FDR < .05). In the *Insular-DMG* cluster, $nCBF_{GM}$ was lower in PT_{PVL} than in PT_H ($p < 0.05$, *p*FDR <0.05) and tended towards a lower value in PT_{GMH} compared to PT_H ($p < .1$, *p*FDR = n.s.). No differences in $nCBF_{GM}$ among groups were identified in the *Parieto-Occipital* and in the *Sensorimotor* clusters.

4 | DISCUSSION

Here, we evaluated the spatial pattern of CBF_{GM} in neonates using pCASL MRI at TEA. Using data-driven hierarchical clustering on normalized (n)CBF_{GM} extracted from 90 ROIs of healthy neonates, we identified 4 groups of brain regions that were labeled *Fronto-Temporal*, *Parieto-Occipital*, *Insular-DGM*, and *Sensorimotor* and were characterized by increasing perfusion.

Comparisons among groups and correlation analysis demonstrated that the $nCBF_{GM}$ varied as a function of GA at birth selectively in the Fronto-Temporal and the Sensorimotor clusters, with a positive and a negative association, respectively. Moreover, the presence of PVL significantly increased the perfusion of *Fronto-Temporal* cluster while decreasing that of *Insular-DGM*. In contrast, GMH appeared to exert a mild perfusion reduction only in the Insular-DGM.

Despite the loss of spatial information in comparison to a voxel-wise or standalone ROI-wise analyses, the advantages of combining the ROI-wise analysis with the clustering approach were twofold. First, despite we implemented a state-of-the-art co-registration approach, the use of large ROIs minimized the effects of residual co-registration errors deriving from the relevant anatomical variability typical of the examined population. Second, the present approach increased data interpretability and statistical power. From a clinical perspective it must be noted that PT newborns show different degrees of impairments in multiple neurocognitive domains, suggesting that wide regions of the brain are affected rather than a specific cortical area. The clustering approach is expected help combine functionally related brain regions that are involved in the impaired functions.

4.1 | Average perfusion pattern in healthy neonates

Our results are consistent with previous studies in neonates indicating higher CBF and metabolic activity in the sensorimotor cortex and the deep GM and lower CBF in higher-order regions (Chugani, 2018; De Vis et al., 2013; Ouyang et al., 2017). This pattern reflects the hierarchical order of development starting in primary cortical areas and

proceeding to unimodal and transmodal associative cortices, which is genetically programmed (Silbereis et al., 2016).

Differently from past results reporting the highest perfusion in the deep GM nuclei (Tortora et al., 2017), we showed that the *Insular-DGM* had a lower perfusion compared to the *Sensorimotor* cluster. We speculate that previous studies might have underestimated the perfusion of the sensorimotor cortices by including them in larger frontal and parietal ROIs.

Interestingly, the *Insular-DGM* cluster also comprised the insula and the auditory cortex in accordance with the notion that both regions are functionally active by the 28th week of GA (Graven & Browne, 2008). Instead, the calcarine cortex (primary visual area) was grouped under the hypoperfused *Parieto-Occipital* cluster. Counterintuitively, occipital CBF was found to be consistently low across different perfusion imaging modalities (Borch & Greisen, 1998; Ouyang et al., 2017). As proposed by Ouyang et al., scanning newborns during sleep, thereby in absence of visual stimuli, may have contributed to the hypo-perfusion of this area (Ouyang et al., 2017).

4.2 | Effects of prematurity on perfusion pattern

We found significant effects of prematurity on relative perfusion within the identified clusters in healthy newborns. Of note, the ascending order of the average perfusion from the fronto-temporal to the sensori-motor cluster was maintained in the different WHO subgroups considered (PT_{HE}, PT_{HM}, PT_{HL}, FT), in accordance with the genetically determined hierarchical trajectory of maturation of different brain regions (Shaw et al., 2008), thus, justifying our clustering approach that combined all healthy neonates in one group.

The *Sensorimotor cluster* showed a negative association between GA at birth and $nCBF_{GM}$. This finding could be the result of the experience-dependent development determined by the longer exposure to extrauterine environment with decreasing GA at birth, particularly in brain regions controlling basic sensorimotor functions, mostly stimulated soon after birth (Bouyssi-Kobar et al., 2018; Jha et al., 2019).

The opposite was found in the *Fronto-Temporal cluster*, which showed higher $nCBF_{GM}$ with increasing GA at birth. We hypothesize that the effects of extra-uterine exposure on regions known to have a late and extended developmental window, such as the prefrontal cortex, may be minimal, thus, explaining their relative hypo-perfusion. In particular, the cause of this hypoperfusion in the associative cortices of healthy PTs could be their relative structural and functional immaturity, as PTs lag behind their FT peers in the processes that sustain cortical thickness and maturation. In these processes, astrocytes play a role as critical regulators of synapse formation, maintenance and refinement (Chung et al., 2013). In the absence of structural damage, prematurity seems to selectively affect astrocyte maturation in the prefrontal cortex. As a consequence, PTs may exhibit a lower number of functioning synapses around TEA as compared to their FT peers, potentially explaining their greater hypoperfusion in the *Fronto-Temporal* cluster (Lacaille et al., 2021). Supporting this interpretation, adult studies reported the presence of thinner cortices in the frontal, temporal, and parietal associative areas of individuals born PT but without overt brain injury (Schmitz-Koep et al., 2020; Zubiaurre-Elorza et al., 2012).

The perfusion of *Parieto-Occipital* and *Insular-DGM* clusters seems to be unaffected by GA at birth. This feature is not new (Tortora et al., 2017): being ontogenetically older, DGM may be less influenced by experience-dependent development and GA at birth.

4.3 | Effects of prematurity-related brain injury on perfusion pattern

PVL and GMH, although different in their pathogenesis and timing, both produce perfusion changes in the GM (Tortora et al., 2017; Tortora et al., 2020). PVL was associated with a significant redistribution of perfusion from a less perfused *Insular-DGM* towards a more perfused *Fronto-Temporal* cluster compared to healthy neonates. In contrast, GMH was associated with a more limited effect in terms of both entity and spatial extent, with a tendency towards a lower perfusion and a more selective involvement of the *Insular-DGM* cluster.

Although both PVL and GMH have a negative trophic effect on cortical and subcortical GM, the effects of PVL on the developing brain are more pleiotropic and far reaching than GMH, possibly indicating that PVL elicits a more severe response of the microglia (Ball et al., 2013; Ortinau & Neil, 2015; Pierson et al., 2007). Indeed, recent molecular studies on Osteopontin (a protein involved in white matter damage/repair) in prematurity-related brain injury showed that there were fewer reactive astrocytes in GMH compared to PVL and that Osteopontin was not expressed in hemorrhage regions (Nilsson et al., 2021). This suggests that PVL evokes a more intense inflammatory response compared to GMH, having more disruptive - and possibly longer lasting - effects on white matter integrity and, in turn, on the developing cortex.

Although the most impaired regions in terms of volumetric decrements and reduced perfusion are those localized adjacent to the PVL lesions (such as those within our *Insular-DGM* cluster), it is possible that the farthest and later-developing ones (i.e., those in our *Fronto-Temporal* cluster) could be affected by post-injury reorganization (Bouyssi-Kobar et al., 2018; Marin-Padilla, 1999). Indeed, thicker associative frontal and temporal cortices were observed in PT children and adolescents with PVL (Nagy et al., 2011; Zubiaurre-Elorza et al., 2012). We speculate that an abnormal or pathologically delayed pruning program might characterize these cortical areas, possibly representing the structural correlate of our metabolic finding.

Another hypothesis is that the relative increase in perfusion in the *Fronto-Temporal* cluster is a consequence of disturbed GABAergic transmission, GABA being a contributor to cortical vessel tone and CBF regulation (Anenberg et al., 2015; Cauli et al., 2004; Uhlirova et al., 2016). The associative cortices are prominent areas for GABA circuitry formation during late gestation, making them particularly vulnerable to alterations in the number of GABA-interneurons (Xu et al., 2011) which are the preferential target of PVL. The reduction of

the GABAergic neurons may thus cause a local increase in CBF. Our hypothesis may be supported by preclinical and post-mortem studies which demonstrated a loss of GABA interneurons in PT infants suffering from hypoxic injury (Robinson et al., 2006; Stevens et al., 2013). However, we acknowledge that this hypothesis remains speculative and warrants further investigations.

4.4 | Study limitations and future perspectives

The present study has some limitations. First, the lack of a subject-specific estimate of the $T1_b$ did not allow the comparison of quantitative CBF among subjects and groups. $T1_b$ is strongly dependent on hematocrit, which is highly variable in neonates (28%–67%) and fluctuates with gestational and postnatal age (De Vis et al., 2014). This problem was tackled in previous studies by inferring the $T1_b$ from capillary-drawn hematocrit values. However, De Vis et al. demonstrated the unreliability of this method (De Vis et al., 2014). Other studies used a standard $T1_b$ for the quantification of CBF, but this method neglects the inter-subject variability of $T1_b$ preventing the accurate CBF comparison among subjects or groups (Bouyssi-Kobar et al., 2018; Mahdi et al., 2018). The estimation of a subject-specific $T1_b$ would thus be ideal in the future, either as a function of subject's hematocrit derived from an arterial blood sample or with a $T1_b$-mapping method (De Vis et al., 2014; Varela et al., 2011). Our study addressed this issue by focusing on the spatial distribution of perfusion through normalization of CBF maps (z-scoring). However, the limitation of this approach is the insensitivity to differences in global CBF, which should be assessed in future studies.

Second, we acknowledge that, given their reduced blood velocity, newborns tend to have a longer ASL bolus arrival time to the brain tissue, accounting for potential underestimation of CBF when using a single PLD. This effect is stronger when using PLDs that are too short to allow the bolus to be completely delivered to the brain. Following established guidelines (Alsop et al., 2015), we set a relatively long PLD suited to probe newborns (PLD = 2 s). Moreover, the spatial normalization that we performed accounted for variability in the average ATT among newborns. However, some residual regional effects of local ATT on CBF may still be present. Future studies could overcome this limitation using multi-PLD ASL.

A third potential limitation is Midazolam use during the scan. General anesthetic agents are commonly used to facilitate pediatric MRI investigations. However, they cause small alterations in brain hemodynamics, particularly midazolam induces a general reduction of CBF (Wang et al., 2020). Nonetheless, the use of sedation cannot explain the group differences observed in the present study, as Midazolam was administered to all newborns.

Fourth, the limited sample size of PTs with brain injury may have reduced the identification of subtle group differences, especially in the GMH subgroup. Therefore, it will be important to validate our findings in a larger cohort of PT infants with GMH and PVL.

In addition, the cross-sectional nature of the study limits our ability to encompass the whole developmental trajectory of the CBF pattern and to establish a causal relationship between structure and function. Future longitudinal studies would shed light on the temporal evolution of the effects and on the role of environmental factors, eventually allowing the identification of the optimal timing of specific targets for therapeutic interventions aimed at improving later cognitive and motor skills of PT infants.

The spatial distribution of CBF could represent an early imaging biomarker of adverse future neurocognitive development. In this respect, the lack of a clinical follow-up represents a further limitation of the present study.

These limitations notwithstanding, our results establish that the distribution of CBF in FT and PT infants around term follows a defined pattern and is differentially affected by prematurity and prematurity-related brain injury. The methodology represents a promising approach to the identification of abnormal patterns of cerebral perfusion. Further work will enable a better characterization of the relationship between spatial distribution of CBF and long-term neurodevelopmental outcome and the utility of pCASL as a noninvasive tool to facilitate accurate stratification of individuals at risk of domain-specific impairments.

AUTHOR CONTRIBUTIONS

Eleonora Piccirilli: Conceptualization, Investigation, Formal analysis, Visualization, Writing–original draft. **Antonio M. Chiarelli:** Conceptualization, Funding acquisition, Formal analysis, Visualization, Writing–original draft. **Carlo Sestieri:** Funding acquisition, Writing– review & editing. **Daniele Mascali**: Formal Analysis. **Darien Calvo Garcia**: Investigation, Data collection. **Adele Primavera**: Data collection. **Rita Salomone**: Data collection. **Richard G. Wise:** Funding acquisition, Visualization, Writing—review & editing. **Antonio Ferretti:** Conceptualization, Funding acquisition, Investigation, Visualization, Writing–review & editing, **Massimo Caulo:** Conceptualization, Funding acquisition, Supervision, Investigation, Visualization, Writing—review & editing.

ACKNOWLEDGMENTS

We thank the families who took part in the study. This work was partially conducted under the framework of the "Departments of Excellence 2018–2022" initiative of the Italian Ministry of Education, University and Research for the Department of Neuroscience, Imaging and Clinical Sciences (DNISC), University of Chieti-Pescara, Italy.

CONFLICT OF INTEREST STATEMENT

Authors declare no competing financial and nonfinancial interests.

DATA AVAILABILITY STATEMENT

Data of the present study are available upon reasonable request.

ORCID

Antonio M. Chiarelli https://orcid.org/0000-0002-5347-8417

REFERENCES

Alsop, D. C., Detre, J. A., Golay, X., Gunther, M., Hendrikse, J., Hernandez-Garcia, L., Lu, H., MacIntosh, B. J., Parkes, L. M., Smits, M., van Osch, M. J. P., Wang, D. J. J., Wong, E. C., & Zaharchuk, G. (2015).

Recommended implementation of arterial spin-labeled perfusion MRI for clinical applications: A consensus of the ISMRM perfusion study group and the European consortium for ASL in dementia. *Magnetic Resonance in Medicine*, *73*(1), 102–116. https://doi.org/10.1002/mrm.25197

Anenberg, E., Chan, A. W., Xie, Y., LeDue, J. M., & Murphy, T. H. (2015). Optogenetic stimulation of GABA neurons can decrease local neuronal activity while increasing cortical blood flow. *Journal of Cerebral Blood Flow and Metabolism*, *35*(10), 1579–1586. https://doi.org/10.1038/jcbfm.2015.140

Avants, B., Tustison, N., Song, G., Yushkevich, P., Song, Z., & Gee, J. (2009). Advanced Normalization Tools: V1. 0. The Insight Journal. Revision, 1, 681.

Avants, B. B., Tustison, N. J., Song, G., Cook, P. A., Klein, A., & Gee, J. C. (2011). A reproducible evaluation of ANTs similarity metric performance in brain image registration. *NeuroImage*, *54*(3), 2033–2044.

Ball, G., Boardman, J. P., Aljabar, P., Pandit, A., Arichi, T., Merchant, N., Rueckert, D., Edwards, A. D., & Counsell, S. J. (2013). The influence of preterm birth on the developing thalamocortical connectome. *Cortex*, *49*(6), 1711–1721. https://doi.org/10.1016/j.cortex.2012.07.006

Borch, K., & Greisen, G. (1998). Blood flow distribution in the normal human preterm brain. *Pediatric Research*, *43*(1), 28–33. https://doi.org/10.1203/00006450-199801000-00005

Bouyssi-Kobar, M., du Plessis, A. J., McCarter, R., Brossard-Racine, M., Murnick, J., Tinkleman, L., Robertson, R. L., & Limperopoulos, C. (2016). Third trimester brain growth in preterm infants compared with In utero healthy fetuses. *Pediatrics*, *138*(5), e20161640. https://doi.org/10.1542/peds.2016-1640

Bouyssi-Kobar, M., Murnick, J., Brossard-Racine, M., Chang, T., Mahdi, E., Jacobs, M., & Limperopoulos, C. (2018). Altered cerebral perfusion in infants born preterm compared with infants born full term. *The Journal of Pediatrics*, *193*, 54–61.e2.

Cauli, B., Tong, X. K., Rancillac, A., Serluca, N., Lambolez, B., Rossier, J., & Hamel, E. (2004). Cortical GABA interneurons in neurovascular coupling: Relays for subcortical vasoactive pathways. *The Journal of Neuroscience*, *24*(41), 8940–8949. https://doi.org/10.1523/JNEUROSCI.3065-04.2004

Chugani, H. T. (2018). Imaging brain metabolism in the newborn. *Journal of Child Neurology*, *33*(13), 851–860. https://doi.org/10.1177/0883073818792308

Chung, W. S., Clarke, L. E., Wang, G. X., Stafford, B. K., Sher, A., Chakraborty, C., Joung, J., Foo, L. C., Thompson, A., Chen, C., Smith, S. J., & Barres, B. A. (2013). Astrocytes mediate synapse elimination through MEGF10 and MERTK pathways. *Nature*, *504*(7480), 394–400. https://doi.org/10.1038/nature12776

De Vis, J. B., Hendrikse, J., Groenendaal, F., de Vries, L. S., Kersbergen, K. J., Benders, M. J., & Petersen, E. T. (2014). Impact of neonate haematocrit variability on the longitudinal relaxation time of blood: Implications for arterial spin labelling MRI. *Neuroimage Clin*, *4*, 517–525. https://doi.org/10.1016/j.nicl.2014.03.006

De Vis, J. B., Petersen, E. T., de Vries, L. S., Groenendaal, F., Kersbergen, K. J., Alderliesten, T., Hendrikse, J., & Benders, M. J. (2013). Regional changes in brain perfusion during brain maturation measured non-invasively with arterial spin labeling MRI in neonates. *European Journal of Radiology*, *82*(3), 538–543. https://doi.org/10.1016/j.ejrad.2012.10.013

Fyfe, K. L., Yiallourou, S. R., Wong, F. Y., & Horne, R. S. (2014). The development of cardiovascular and cerebral vascular control in preterm infants. *Sleep Medicine Reviews*, *18*(4), 299–310. https://doi.org/10.1016/j.smrv.2013.06.002

Graven, S. N., & Browne, J. V. (2008). Auditory development in the fetus and infant. *Newborn and Infant Nursing Reviews*, *8*(4), 187–193.

Hesterberg, T. (2011). Bootstrap. *Wiley Interdisciplinary Reviews: Computational Statistics*, *3*(6), 497–526.

Jenkinson, M., Beckmann, C. F., Behrens, T. E., Woolrich, M. W., & Smith, S. M. (2012). FSL. *Neuroimage*, *62*(2), 782–790. https://doi.org/10.1016/j.neuroimage.2011.09.015

Jha, S. C., Xia, K., Ahn, M., Girault, J. B., Li, G., Wang, L., Shen, D., Zou, F., Zhu, H., Styner, M., Gilmore, J. H., & Knickmeyer, R. C. (2019). Environmental influences on infant cortical thickness and surface area. *Cerebral Cortex*, *29*(3), 1139–1149. https://doi.org/10.1093/cercor/bhy020

Kidokoro, H., Anderson, P. J., Doyle, L. W., Woodward, L. J., Neil, J. J., & Inder, T. E. (2014). Brain injury and altered brain growth in preterm infants: Predictors and prognosis. *Pediatrics*, *134*(2), e444–e453. https://doi.org/10.1542/peds.2013-2336

Kim, H. G., Lee, J. H., Choi, J. W., Han, M., Gho, S. M., & Moon, Y. (2018). Multidelay arterial spin-labeling MRI in neonates and infants: Cerebral perfusion changes during brain maturation. *AJNR. American Journal of Neuroradiology*, *39*(10), 1912–1918. https://doi.org/10.3174/ajnr.A5774

Lacaille, H., Vacher, C. M., & Penn, A. A. (2021). Preterm birth alters the maturation of the GABAergic system in the human prefrontal cortex. *Frontiers in Molecular Neuroscience*, *14*, 827370. https://doi.org/10.3389/fnmol.2021.827370

Leijser, L. M., Srinivasan, L., Rutherford, M. A., van Wezel-Meijler, G., Counsell, S. J., Allsop, J. M., & Cowan, F. M. (2009). Frequently encountered cranial ultrasound features in the white matter of preterm infants: Correlation with MRI. *European Journal of Paediatric Neurology*, *13*(4), 317–326.

Lubsen, J., Vohr, B., Myers, E., Hampson, M., Lacadie, C., Schneider, K. C., Katz, K. H., Constable, R. T., & Ment, L. R. (2011). Microstructural and functional connectivity in the developing preterm brain. *Seminars in Perinatology*, *35*(1), 34–43. https://doi.org/10.1053/j.semperi.2010.10.006

Mahdi, E. S., Bouyssi-Kobar, M., Jacobs, M. B., Murnick, J., Chang, T., & Limperopoulos, C. (2018). Cerebral perfusion is perturbed by preterm birth and brain injury. *AJNR. American Journal of Neuroradiology*, *39*(7), 1330–1335. https://doi.org/10.3174/ajnr.A5669

Makropoulos, A., Robinson, E. C., Schuh, A., Wright, R., Fitzgibbon, S., Bozek, J., Counsell, S. J., Steinweg, J., Vecchiato, K., Passerat-Palmbach, J., Lenz, G., Mortari, F., Tenev, T., Duff, E. P., Bastiani, M., Cordero-Grande, L., Hughes, E., Tusor, N., Tournier, J. D., … Rueckert, D. (2018). The developing human connectome project: A minimal processing pipeline for neonatal cortical surface reconstruction. *NeuroImage*, *173*, 88–112. https://doi.org/10.1016/j.neuroimage.2018.01.054

Marin-Padilla, M. (1999). Developmental neuropathology and impact of perinatal brain damage. III: Gray matter lesions of the neocortex. *Journal of Neuropathology and Experimental Neurology*, *58*(5), 407–429. https://doi.org/10.1097/00005072-199905000-00001

Mukerji, A., Shah, V., & Shah, P. S. (2015). Periventricular/intraventricular hemorrhage and neurodevelopmental outcomes: A meta-analysis. *Pediatrics*, *136*(6), 1132–1143. https://doi.org/10.1542/peds.2015-0944

Nagy, Z., Lagercrantz, H., & Hutton, C. (2011). Effects of preterm birth on cortical thickness measured in adolescence. *Cerebral Cortex*, *21*(2), 300–306. https://doi.org/10.1093/cercor/bhq095

Nilsson, G., Baburamani, A. A., Rutherford, M. A., Zhu, C., Mallard, C., Hagberg, H., Vontell, R., & Wang, X. (2021). White matter injury but not germinal matrix hemorrhage induces elevated osteopontin expression in human preterm brains. *Acta Neuropathologica Communications*, *9*(1), 166. https://doi.org/10.1186/s40478-021-01267-7

Ortinau, C., & Neil, J. (2015). The neuroanatomy of prematurity: Normal brain development and the impact of preterm birth. *Clinical Anatomy*, *28*(2), 168–183. https://doi.org/10.1002/ca.22430

Ouyang, M., Liu, P., Jeon, T., Chalak, L., Heyne, R., Rollins, N. K., Licht, D. J., Detre, J. A., TPL, R., Lu, H., & Lu, H. (2017). Heterogeneous increases of regional cerebral blood flow during preterm brain

development: Preliminary assessment with pseudo-continuous arterial spin labeled perfusion MRI. *NeuroImage*, *147*, 233–242.

Padilla, N., Alexandrou, G., Blennow, M., Lagercrantz, H., & Aden, U. (2015). Brain growth gains and losses in extremely preterm infants at term. *Cerebral Cortex*, *25*(7), 1897–1905. https://doi.org/10.1093/cercor/bht431

Pierson, C. R., Folkerth, R. D., Billiards, S. S., Trachtenberg, F. L., Drinkwater, M. E., Volpe, J. J., & Kinney, H. C. (2007). Gray matter injury associated with periventricular leukomalacia in the premature infant. *Acta Neuropathologica*, *114*(6), 619–631. https://doi.org/10.1007/s00401-007-0295-5

Robert, L. T. (1953). Who belongs in the family? *Psychometrika*, *18*(4), 267276.

Robinson, S., Li, Q., DeChant, A., & Cohen, M. L. (2006). Neonatal loss of γ–aminobutyric acid pathway expression after human perinatal brain injury. *Journal of Neurosurgery: Pediatrics*, *104*(6), 396–408.

Schmitz-Koep, B., Bauml, J. G., Menegaux, A., Nuttall, R., Zimmermann, J., Schneider, S. C., Daamen, M., Scheef, L., Boecker, H., Zimmer, C., Gaser, C., Wolke, D., Bartmann, P., Sorg, C., & Hedderich, D. M. (2020). Decreased cortical thickness mediates the relationship between premature birth and cognitive performance in adulthood. *Human Brain Mapping*, *41*(17), 4952–4963. https://doi.org/10.1002/hbm.25172

Shaw, P., Kabani, N. J., Lerch, J. P., Eckstrand, K., Lenroot, R., Gogtay, N., Greenstein, D., Clasen, L., Evans, A., Rapoport, J. L., Giedd, J. N., & Wise, S. P. (2008). Neurodevelopmental trajectories of the human cerebral cortex. *The Journal of Neuroscience*, *28*(14), 3586–3594. https://doi.org/10.1523/JNEUROSCI.5309-07.2008

Shi, F., Yap, P. T., Wu, G., Jia, H., Gilmore, J. H., Lin, W., & Shen, D. (2011). Infant brain atlases from neonates to 1- and 2-year-olds. *PLoS One*, *6*(4), e18746. https://doi.org/10.1371/journal.pone.0018746

Silbereis, J. C., Pochareddy, S., Zhu, Y., Li, M., & Sestan, N. (2016). The cellular and molecular landscapes of the developing human central nervous system. *Neuron*, *89*(2), 248–268. https://doi.org/10.1016/j.neuron.2015.12.008

Stevens, H. E., Su, T., Yanagawa, Y., & Vaccarino, F. M. (2013). Prenatal stress delays inhibitory neuron progenitor migration in the developing neocortex. *Psychoneuroendocrinology*, *38*(4), 509–521.

Tortora, D., Lo Russo, F. M., Severino, M., Parodi, A., Massirio, P., Ramenghi, L. A., & Rossi, A. (2020). Regional impairment of cortical and deep gray matter perfusion in preterm neonates with low-grade germinal matrix-intraventricular hemorrhage: An ASL study. *Neuroradiology*, *62*(12), 1689–1699. https://doi.org/10.1007/s00234-020-02514-9

Tortora, D., Mattei, P. A., Navarra, R., Panara, V., Salomone, R., Rossi, A., Detre, J. A., & Caulo, M. (2017). Prematurity and brain perfusion: Arterial spin labeling MRI. *Neuroimage Clin*, *15*, 401–407. https://doi.org/10.1016/j.nicl.2017.05.023

Uhlirova, H., Kilic, K., Tian, P., Thunemann, M., Desjardins, M., Saisan, P. A., Sakadžić, S., Ness, T. V., Mateo, C., Cheng, Q., Weldy, K. L., Razoux, F., Vandenberghe, M., Cremonesi, J. A., Ferri, C. G., Nizar, K., Sridhar, V. B., Steed, T. C., Abashin, M., … Devor, A. (2016). Cell type specificity of neurovascular coupling in cerebral cortex. *eLife*, *5*, e14315. https://doi.org/10.7554/eLife.14315

Varela, M., Hajnal, J. V., Petersen, E. T., Golay, X., Merchant, N., & Larkman, D. J. (2011). A method for rapid in vivo measurement of blood T1. *NMR in Biomedicine*, *24*(1), 80–88. https://doi.org/10.1002/nbm.1559

Wang, J., Sun, P., & Liang, P. (2020). Neuropsychopharmacological effects of midazolam on the human brain. *Brain Informatics*, *7*(1), 1–12.

Ward, J. H., Jr. (1963). Hierarchical grouping to optimize an objective function. *Journal of the American Statistical Association*, *58*(301), 236–244.

Woodward, L. J., Clark, C. A., Bora, S., & Inder, T. E. (2012). Neonatal white matter abnormalities an important predictor of neurocognitive outcome for very preterm children. *PLoS One*, *7*(12), e51879. https://doi.org/10.1371/journal.pone.0051879

World Health Organization. (2012). *Born too soon: The global action report on preterm birth*. World Health Organization.

Xu, G., Broadbelt, K. G., Haynes, R. L., Folkerth, R. D., Borenstein, N. S., Belliveau, R. A., Trachtenberg, F. L., Volpe, J. J., & Kinney, H. C. (2011). Late development of the GABAergic system in the human cerebral cortex and white matter. *Journal of Neuropathology and Experimental Neurology*, *70*(10), 841–858. https://doi.org/10.1097/NEN.0b013e31822f471c

Zubiaurre-Elorza, L., Soria-Pastor, S., Junque, C., Sala-Llonch, R., Segarra, D., Bargallo, N., & Macaya, A. (2012). Cortical thickness and behavior abnormalities in children born preterm. *PLoS One*, *7*(7), e42148. https://doi.org/10.1371/journal.pone.0042148

Zun, Z., Kapse, K., Jacobs, M., Basu, S., Said, M., Andersen, N., Murnick, J., Chang, T., du Plessis, A., & Limperopoulos, C. (2021). Longitudinal trajectories of regional cerebral blood flow in very preterm infants during third trimester ex utero development assessed with MRI. *Radiology*, *299*(3), 691–702. https://doi.org/10.1148/radiol.2021202423

SUPPORTING INFORMATION

Additional supporting information can be found online in the Supporting Information section at the end of this article.

How to cite this article: Piccirilli, E., Chiarelli, A. M., Sestieri, C., Mascali, D., Calvo Garcia, D., Primavera, A., Salomone, R., Wise, R. G., Ferretti, A., & Caulo, M. (2023). Cerebral blood flow patterns in preterm and term neonates assessed with pseudo-continuous arterial spin labeling perfusion MRI. *Human Brain Mapping*, 1–12. https://doi.org/10.1002/hbm.26315